IEEE Photonics Journal
An IEEE Photonics Society Publication

Open Access

Coherent and Incoherent Nonparaxial Self-Accelerating Weber Beams

Volume 8, Number 6, December 2016

Yiqi Zhang
Junfeng Liu
Feng Wen
Changbiao Li
Zhaoyang Zhang
Yanpeng Zhang
Milivoj R. Belić

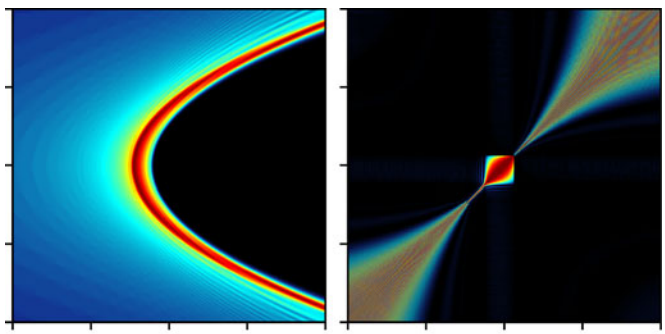

DOI: 10.1109/JPHOT.2016.2620809
1943-0655 © 2016 IEEE

IEEE photonics SOCIETY

IEEE

Coherent and Incoherent Nonparaxial Self-Accelerating Weber Beams

Yiqi Zhang,[1,2] Junfeng Liu,[1] Feng Wen,[1,2] Changbiao Li,[1,2] Zhaoyang Zhang,[1,2] Yanpeng Zhang,[1] and Milivoj R. Belić[3]

[1]Key Laboratory for Physical Electronics and Devices of the Ministry of Education and Shaanxi Key Lab of Information Photonic Technique, Xi'an Jiaotong University, Xi'an 710049, China
[2]Department of Applied Physics, School of Science, Xi'an Jiaotong University, Xi'an 710049, China
[3]Science Program, Texas A&M University at Qatar, Doha 23874, Qatar

DOI:10.1109/JPHOT.2016.2620809

Manuscript received October 6, 2016; accepted October 20, 2016. Date of current version November 7, 2016. This work was supported in part by the National Basic Research Program of China under Grant 2012CB921804; in part by the National Natural Science Foundation of China under Grant 61308015, Grant 11474228, and Grant 61605154; in part by the Key Scientific and Technological Innovation Team of Shaanxi Province (2014KCT-10); and in part by the Qatar National Research Fund (NPRP 6-021-1-005). The work of M. R. Belić was also supported by the Al Sraiya Holding Group. Corresponding authors: Yiqi Zhang (e-mail: zhangyiqi@mail.xjtu.edu.cn), Yanpeng Zhang (e-mail: ypzhang@mail.xjtu.edu.cn), and Milivoj R. Belić (e-mail: milivoj.belic@qatar.tamu.edu).

Abstract: We investigate coherent and incoherent nonparaxial Weber beams both theoretically and numerically. We clarify the understanding of coherence properties of Weber beams. We show that the superposition of coherent self-accelerating Weber beams with transverse displacement cannot display the nonparaxial accelerating Talbot effect because their lobes do not accelerate in unison, which is the requirement for the appearance of the effect. The incoherent Weber beams also cannot display the accelerating Talbot effect but can exhibit nonparaxial accelerating properties, although the transverse coherence length is smaller than the beam width, based on the second-order coherence theory. Our research method applies to the nonparaxial Mathieu beams as well, and one obtains similar conclusions as for the Weber beams, although this is not discussed in the paper.

Index Terms: Weber beams, Talbot effect, incoherent beams.

1. Introduction

The paraxial wave propagation equation is formally equivalent to the Schrödinger equation in quantum mechanics [1], which historically has helped a lot in the discovery of nondiffracting self-accelerating Airy beams [2], [3]. Over the past decade, investigations into the topic have been many and have acquired a rapid development. Until now, studies of Airy beams have been reported in nonlinear media [4]–[7], optical fibers [8], [9], and other systems. To manipulate the behavior of Airy beams, different external potentials, such as harmonic potential [10]–[12] or a linear potential [13], [14], have been explored. Other paraxial and nonparaxial accelerating beams followed soon after.

To recall, the paraxial wave propagation results from Maxwell's equations, after applying the slowly-varying envelope approximation. Without such an approximation, one investigates nonparaxial optical beams using the Helmholtz equation that follows directly from the Maxwell's equations [15]. It has been demonstrated that the solutions of the two-dimensional (2-D) Helmholtz

equation are plane waves in Cartesian coordinates, Bessel beams in polar coordinates [16]–[20], Mathieu beams in elliptic coordinates [21], [22], and Weber beams in parabolic coordinates [21], [23]–[26]. In addition to the 2-D case, one can also solve the 3-D Helmholtz equation for the 3-D accelerating beams by, e.g., utilizing the Whittaker integral [16], [27], [28]. In 3-D, one proceeds to the separation of variables in the Helmholtz equation, expressed in the corresponding coordinate systems; Cartesian, cylindrical, elliptic cylindrical, or parabolic cylindrical. There also exist more exotic patterns [29]–[31] that cannot be directly associated with the separation of variables in the Helmholtz equation. Indeed, there were quite a few interesting results related to the nonparaxial accelerating propagation of this kind that appeared recently in the literature [32]–[34]. The reason why investigations of accelerating beams are so hot at the moment is their numerous potential applications, such as particle manipulation [35]–[37], electron beam shaping [38], and super-resolution imaging [39], to name a few. Recent studies indicated that accelerating beams have opened a new window in explorations of elusive problems in general relativity [40], [41] and exotic quantum particles [42]. For more details on accelerating beams, see review articles [43]–[46] and references therein.

In this paper, we investigate the coherent and incoherent nonparaxial accelerating Weber beams. We focus on the two aspects: 1) Can coherent Weber beams exhibit nonparaxial accelerating Talbot effect, as Bessel beams do, and 2) what behavior will incoherent Weber beams display? Will they lose the nonparaxial accelerating property? The organization of the article is as follows. In Section 2, we introduce the theoretical model and the Weber beams in parabolic coordinates. In Section 3, we investigate the coherent Weber beams and check whether the nonparaxial accelerating Talbot effect can take place or not. In Section 4, incoherent Weber beams and their characterization are considered, including the degree of coherence and the coherence length. We conclude the article in Section 5.

2. Theoretical Model

We begin from the 2-D Helmholtz equation, which can be written as

$$\left(\frac{\partial^2}{\partial x^2}+\frac{\partial^2}{\partial z^2}\right)\psi+ k^2\psi = 0 \tag{1}$$

where k is the wavenumber. One of the shape-preserving solutions of (1) is the so-called Weber wave function in the parabolic coordinates. The transformation between Cartesian coordinates (x, z) and parabolic coordinates (η, ξ) is accomplished by the relation $x + iz = (\eta + i\xi)^2/2$, with $\eta \in (-\infty, \infty)$ and $\xi \in [0, \infty)$. By utilizing variable separation, that is, by writing the solution of (1) as $\psi(\xi, \eta) = R(\xi)\Phi(\eta)$, one obtains two ordinary differential equations [21]–[26]:

$$\frac{\partial^2 R(\xi)}{\partial \xi^2}+\left(k^2\xi^2-2ka\right)R(\xi)=0 \tag{2a}$$

$$\frac{\partial^2 \Phi(\eta)}{\partial \eta^2}+\left(k^2\eta^2+2ka\right)\Phi(\eta)=0 \tag{2b}$$

where $2ka$ is the separation constant. The parameter a affects both the scaling and the curvature of parabolic lobes of the Weber beam, as it will be discussed in the following text. If one sets $\sqrt{2k}\xi = v$ and $\sqrt{2k}\eta = u$, (2a) and (2b) transform into the canonical form of the parabolic cylinder differential equations

$$\frac{\partial^2 R(v)}{\partial u^2}+\left(\frac{v^2}{4}-a\right)R(v)=0 \tag{3a}$$

$$\frac{\partial^2 \Phi(u)}{\partial v^2}+\left(\frac{u^2}{4}+a\right)\Phi(u)=0. \tag{3b}$$

The solutions of (2a) and (2b) are determined by the same Weber functions, but the corresponding eigenvalues have opposite signs. If we denote the even and odd solutions of (2a) as P_e and P_o, the final even and odd transverse stationary solutions of (1) in parabolic coordinates are expressed as

$$W_e(x, z; a) = \frac{1}{\sqrt{2\pi}}|\Gamma_1|^2 P_e\left(\sqrt{2k}\xi; a\right) P_e\left(\sqrt{2k}\eta; -a\right) \tag{4a}$$

$$W_o(x, z; a) = \frac{2}{\sqrt{2\pi}}|\Gamma_3|^2 P_o\left(\sqrt{2k}\xi; a\right) P_o\left(\sqrt{2k}\eta; -a\right) \tag{4b}$$

respectively, where

$$P_{e,o}(t, a) = \sum_{n=0}^{\infty} c_n \frac{t^n}{n!}. \tag{5}$$

$\Gamma_1 = \Gamma[(1/4) + (1/2)ia]$, $\Gamma_3 = \Gamma[(3/4) + (1/2)ia]$, and the coefficients c_n satisfy the following recurrence relation:

$$c_{n+2} = ac_n - \frac{n(n-1)c_{n-2}}{4}. \tag{6}$$

For P_e (P_o), the first two coefficients are $c_0 = 1$ and $c_1 = 0$ ($c_0 = 0$ and $c_1 = 1$) [23]. Plugging (5) and (6) into (4a) and (4b) allows the determination of even and odd Weber solutions. Therefore, the transverse stationary solution of (1) can be written in the form

$$W(x, z; a) = W_e(x, z; a) + iW_o(x, z; a), \tag{7}$$

in which rapid intensity modulations along each parabolic lobe are avoided.

According to [26], if $a \geq 10$, the trajectory of the main lobe of the Weber beam in (7) is of the form

$$x = \frac{1}{2f(a)}z^2 - \frac{1}{2}f(a) \tag{8}$$

where

$$f(a) \approx \frac{1}{2k}\left(2\sqrt{a} + \frac{0.9838}{\sqrt[25]{a^4}}\right)^2.$$

Clearly, the trajectory in (8) is a parabolic curve that depends on the value of a. Therefore, if one fixes the value of a, then the trajectory is also determined regardless of whether there is a transverse displacement or not.

To elucidate Weber beams more clearly, we display in Fig. 1 the intensity distributions of the even, odd and general transverse stationary solutions of the corresponding Helmholtz equation. In Fig. 1(c), the theoretical trajectory of the main lobe is also exhibited, as indicated by the dashed curve. However, it should be stressed that lobes of the Weber beam do not accelerate in unison. That is, the path differences along different lobe trajectories vary such that they are not uniform and fixed. This is unlike the nonparaxial Bessel beams, where the lobes follow circular trajectories. The rate of change of the path length with the radial distance there is constant. A more clear sketch of the Weber beam is displayed in Fig. 1(d), in which the transverse coordinate is transformed according to (8) that describes the trajectory of the main lobe. One sees that all lobes except the main lobe do not propagate along a straight trajectory.

In addition to the analytical form in (7), one can display a simple Weber beam numerically, using the Helmholtz equation (1) directly. In Fig. 2(a), we show the numerically obtained propagation of a Weber beam, i.e. the beam at $z = 0$ of Fig. 1(c). One can see that it is in accordance with the analytical result. To check the self-healing effect of the Weber beam, we remove the main lobe of an input Weber beam, and display the propagation of the remainder in Fig. 2(b). One sees that the main lobe has recovered during propagation, and the self-healing effect is evident [26].

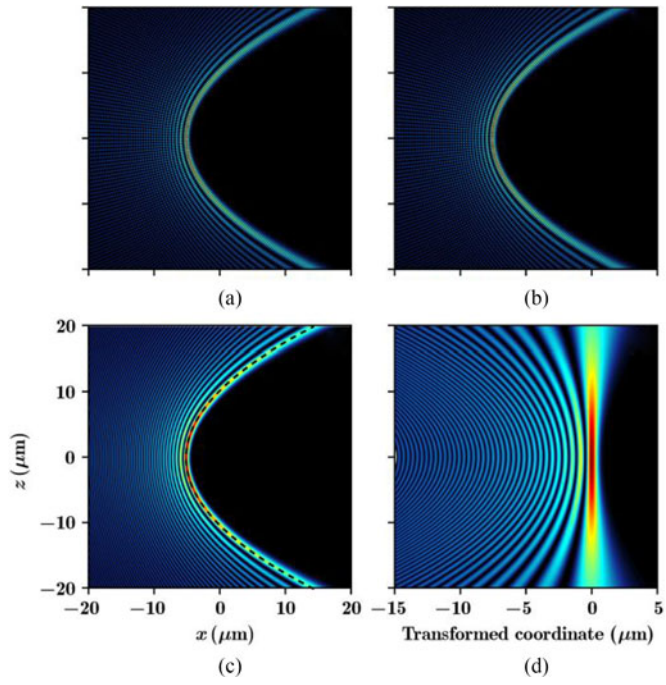

Fig. 1. Intensity distributions of the even (a), odd (b), and general (c) transverse stationary Weber solutions. The dashed curve in (c) is the theoretical trajectory of the main lobe. (d) Same as (c), but the transverse coordinate is transformed according to (8). (a)-(c) share the same scales, and all the panels share the same vertical scale. Other parameters are $a = 50$ and $\lambda = 600\,\text{nm}$.

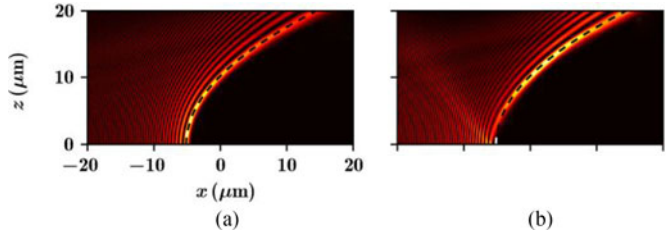

Fig. 2. (a) Numerical propagation of a Weber beam, corresponding to Fig. 1(c). (b) Self-healing of the Weber beam. The main lobe of the beam is blocked at the origin; it recovers fast.

In the following, we discuss the coherent and incoherent Weber beams in more detail, based on the basic theory introduced here. In particular, we discuss whether they can exhibit the nonparaxial accelerating Talbot effect or not.

3. Coherent Weber Beams

Due to the linear property of (1), the solution in (7) with an arbitrary transverse displacement Δx is also a solution.

Thus, the general solution of (1) in parabolic coordinates can be written as

$$W(x, z; a) = \sum_{a\in\mathbb{R}} \sum_{n\in\mathbb{Z}} [W_e(x + n\Delta x, z; a) + iW_o(x + n\Delta x, z; a)] \tag{9}$$

in which the coefficients of all the components are set to 1.

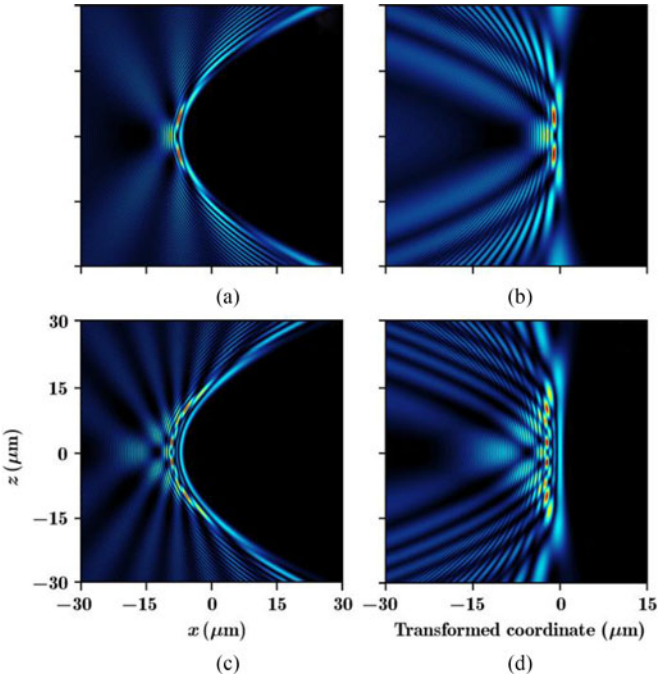

Fig. 3. (a) Intensity distributions of the general nonparaxial Weber beam with two components $n = 0$ and $n = 3$. (b) Same as (a) but with the transverse coordinate transformed. (c) and (d) Setup is in (a) and (b), but for $n = 0$ and $n = 6$. (a) and (c) share the same scale, while (b) and (d) also share the same scale. Other parameters are $a = 70$, $\lambda = 600$ nm, and $\Delta x \approx 39.07$ nm.

Even though the nonparaxial Weber beam can be reduced to the paraxial Airy beam under proper conditions [21], [26], the lobes of the Weber beam do not accelerate in unison, as it is visible in Fig. 1(c) and from the "periodic" Weber beam in [26, Fig. 4(b)]. We would like to explain this in some detail. The parabolic coordinate system is defined by two sets of orthogonal confocal parabolas; one set of parabolas with different latus recti and the separation between the lobes opens upward along the $+x$ axis, and the other opens downward along the $-x$ axis. On the other side, the lobes of Airy beams are governed by a single parabola. A single Airy beam as it propagates maintains its profile within the region of existence, but this is not the case for Weber beams, because their lobes change separation as they propagate.

Since the theoretical trajectory of the main lobe depends on a, the Weber beams with different a do not accelerate in unison. Therefore, we only consider the solution with a fixed a and arbitrary transverse displacement. Then, (9) is reduced to

$$W(x, z; a) = \sum_{n \in \mathbb{Z}} [W_e(x + n\Delta x, z; a) + i W_o(x + n\Delta x, z; a)]. \tag{10}$$

We display the intensity distribution of the beam with only two components given by (10) in Fig. 3(a) and in Fig. 3(b) with a transformed coordinate, according to (8). One finds that the beam exhibits a quasi-periodic behavior along the z direction; however, this pattern cannot be called a Talbot effect [47], [48]. The reason is clear: The lobes do not accelerate in unison, and the unison acceleration is a requirement [17] for the accelerating Talbot effect. What one sees is just the interference pattern of limited periodicity. Another reason is that the intensity and the width of each lobe, respectively, decrease and increase with the increasing propagation distance z, as elucidated in Fig. 1(d). Clearly, the self-imaging properties of the nonparaxial Weber beams are much worse than those of the nonparaxial Bessel beams. In the Bessel beams one can see an extended region in which the nonparaxial Talbot effect is observed. Due to the above reasons, we

assert that one cannot obtain nonparaxial accelerating Talbot effect based on the Weber beams. As a result, different from the nonparaxial Bessel beams [20] and Airy beams [48], the nonparaxial Weber beams do not possess "duality."

Even though one cannot obtain the nonparaxial Talbot effect for Weber beams, there is indeed quasi-periodicity observed in the general transverse stationary solution, caused by interference, and the pattern is also dependent on the transverse displacement Δx. For comparison, we display the quasi-periodic Weber beam in Figs. 3(c) and 3(d) again that corresponds to Figs. 3(a) and 3(b), but with a bigger Δx. One finds that the interference fringes are denser in Figs. 3(c) and 3(d) than those in Figs. 3(a) and 3(b), which indicates the quasi-periodic pattern has a smaller "period" when Δx is larger.

4. Incoherent Weber Beams

For the spatially incoherent case, the intensity of the beam which is composed of an arbitrary number of independent modes, should be written as

$$I(x, z; a) = \sum_{a\in\mathbb{R}} \sum_{n\in\mathbb{Z}} \left| W_e(x + n\Delta x, z; a) + iW_o(x + n\Delta x, z; a) \right|^2 \tag{11}$$

which is different from the coherent case described by (9).

One can check the coherence characteristics of the beam represented in (11) through the complex degree of coherence [49]

$$\gamma_{12}(\vec{r}_1, \vec{r}_2) = \frac{\Gamma(\vec{r}_1, \vec{r}_2)}{\sqrt{I(\vec{r}_1)}\sqrt{I(\vec{r}_2)}} \tag{12}$$

where $\Gamma(\vec{r}_1, \vec{r}_2)$ is the mutual coherence function, defined as

$$\Gamma(\vec{r}_1, \vec{r}_2) = \sum_{n\in\mathbb{Z}} W_n^*(\vec{r}_1) W_n(\vec{r}_2) \tag{13}$$

where W_n represents the beam components and asterisk denotes the complex conjugate. It should be recalled that

$$0 \le |\gamma_{12}(\vec{r}_1, \vec{r}_2)| \le 1 \tag{14}$$

where 0 represents a completely incoherent and 1 a completely coherent beam. Connected with the coherence function, it is also convenient to explore the coherence properties via the transverse coherence length, which is defined as

$$l_c(x) = \int_{-\infty}^{+\infty} \left|\gamma_{12}(x, x')\right|^2 dx'. \tag{15}$$

Based on (11), the intensity of the incoherent Weber beam is shown in Fig. 4(a). Since all the components accelerate along the same trajectory (a parabolic curve with transverse displacements), one can still observe the nonparaxial acceleration property of the incoherent beam, even though the oscillating lobes disappear due to the superposition of incoherent modes. Intensity distributions of the beam at certain distances are displayed as the solid curves in Fig. 4(e), from which one finds that the beam indeed accelerates nonparaxially with a nearly preserved shape. Note that the intensity of the beam depends on the number of modes, and the larger the number, the higher the intensity.

To investigate the incoherence of the beam, in Figs. 4(b)–(d), we present the corresponding complex degree of spatial coherence function, according to (13), at $z = 0$, $z = 10$ μm, and $z = 20$ μm, respectively. The dashed ellipses show the spatial location of the main lobe of the incoherent Weber beam, so that one can numerically find the full width at the half maximum (FWHM) of the main lobe of $|\gamma_{12}|^2$, to characterize the coherence property, which is around several hundreds of nanometers and increases with the propagation distance. From the solid curves in Fig. 4(e),

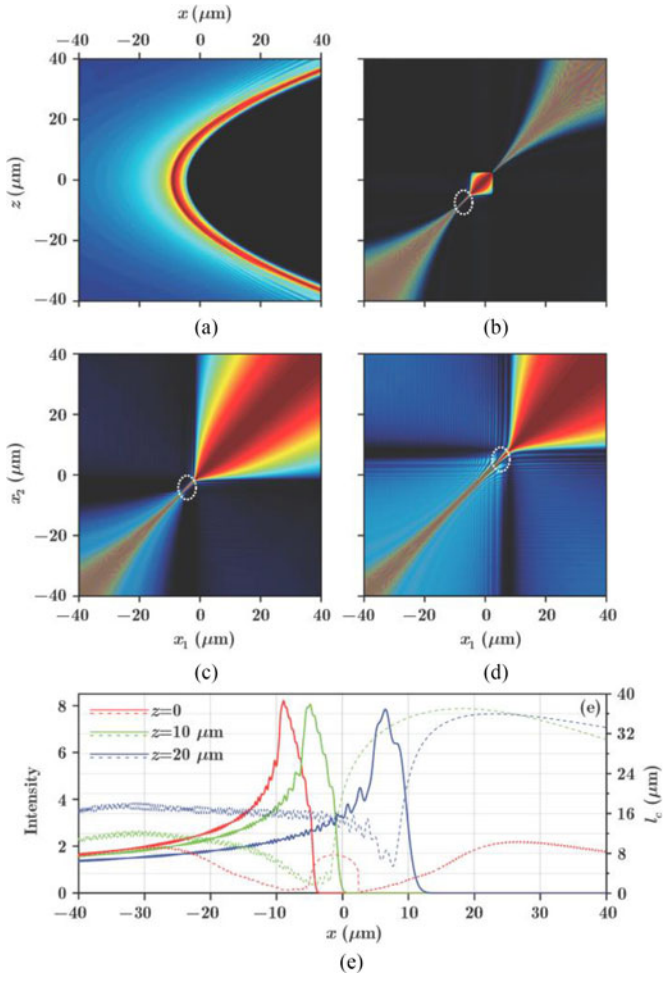

Fig. 4. (a) Intensity distribution of an incoherent Weber beam composed of 129 modes with random transverse displacements in the range $[-2.5, 2.5]$ μm. (b)–(d) Complex degree of spatial coherence function $|\gamma_{12}(x_1, x_2)|^2$ at $z = 0$, $z = 10$ μm, and $z = 20$ μm, respectively. The panels share the same variables and scales. The dotted ellipses indicate the effective regions of the coherence function. (e) Intensity distributions and transverse coherence lengths of the incoherent Weber beam corresponding to (b)–(d). Solid and dashed curves refer to the left and right vertical coordinates and variables, respectively. Other parameters are $a = 70$ and $\lambda = 600$ nm.

one can find that the beam width x_0 of the incoherent Weber beam mostly varies in the region $7\ \mu\text{m} < x_0 < 7.5\ \mu\text{m}$, which is larger than the FWHM of $|\gamma_{12}|^2$.

In the end, we turn to the coherence length, as shown by the dashed curves in Fig. 4(e). Corresponding to the main lobe of the incoherent beam, the coherence length is really small and on the order of a single wavelength (hundreds of nanometers), which is in accordance with the results presented in Figs. 4(b)–(d). One trivial fact worth mentioning is that the incoherence will be strengthened if the transverse displacement extends over a larger region.

5. Conclusion

In conclusion, we have investigated the coherent and partially incoherent Weber beams. For the coherent case, the nonparaxial accelerating Talbot effect cannot be obtained, because the lobes of the Weber beam do not accelerate in unison. For the incoherent case there is still no accelerating Talbot effect, but the beam maintains the nonparaxial accelerating property. Both the coherence function and the coherence length of the beam are presented, to display the degree of coherence,

and we have found that the coherence length is on the order of a micrometer, which is comparable with the wavelength. The method applied to Weber beams is also applicable to coherent and incoherent nonparaxial Mathieu beams, however the Mathieu beams are not discussed here. Nevertheless, similar results are expected. The only difference is that Mathieu beams accelerate along elliptical curves, rather than parabolic, and are solutions of the Helmholtz equation in elliptical coordinates. Last but not least, the self-healing effect still holds for both the coherent and incoherent Weber and Mathieu beams, because they are composed by superpositions of single components that all exhibit the self-healing effect. This presentation enriches the understanding of nonparaxial accelerating beams and the coherence properties of such nonparaxial accelerating light.

Acknowledgment

The authors would like to thank anonymous referees for their useful comments to improve this paper.

References

[1] M. V. Berry and N. L. Balazs, "Nonspreading wave packets," *Amer. J. Phys.*, vol. 47, pp. 264–267, 1979.
[2] G. A. Siviloglou and D. N. Christodoulides, "Accelerating finite energy airy beams," *Opt. Lett.*, vol. 32, pp. 979–981, Apr. 2007.
[3] G. Siviloglou, J. Broky, A. Dogariu, and D. Christodoulides, "Observation of accelerating airy beams," *Phys. Rev. Lett.*, vol. 99, Nov. 2007, Art. no. 213901.
[4] I. Kaminer, M. Segev, and D. N. Christodoulides, "Self-accelerating self-trapped optical beams," *Phys. Rev. Lett.*, vol. 106, May 2011, Art. no. 213903.
[5] I. Dolev, I. Kaminer, A. Shapira, M. Segev, and A. Arie, "Experimental observation of self-accelerating beams in quadratic nonlinear media," *Phys. Rev. Lett.*, vol. 108, Mar. 2012, Art. no. 113903.
[6] Y. Q. Zhang *et al.*, "Soliton pair generation in the interactions of airy and nonlinear accelerating beams," *Opt. Lett.*, vol. 38, pp. 4585–4588, Nov. 2013.
[7] Y. Q. Zhang *et al.*, "Interactions of airy beams, nonlinear accelerating beams, and induced solitons in kerr and saturable nonlinear media," *Opt. Exp.*, vol. 22, pp. 7160–7171, Mar. 2014.
[8] L. Zhang, K. Liu, H. Zhong, J. Zhang, Y. Li, and D. Fan, "Effect of initial frequency chirp on airy pulse propagation in an optical fiber," *Opt. Exp.*, vol. 23, pp. 2566–2576, Feb. 2015.
[9] Y. Hu, A. Tehranchi, S. Wabnitz, R. Kashyap, Z. Chen, and R. Morandotti, "Improved intrapulse Raman scattering control via asymmetric airy pulses," *Phys. Rev. Lett.*, vol. 114, Feb. 2015, Art. no. 073901.
[10] M. A. Bandres and J. C. Gutiérrez-Vega, "Airy-Gauss beams and their transformation by paraxial optical systems," *Opt. Exp.*, vol. 15, pp. 16719–16728, Dec. 2007.
[11] Y. Q. Zhang *et al.*, "Periodic inversion and phase transition of finite energy airy beams in a medium with parabolic potential," *Opt. Exp.*, vol. 23, pp. 10467–10480, Apr. 2015.
[12] Y. Q. Zhang, X. Liu, M. R. Belić, W. P. Zhong, M. S. Petrovi´c, and Y. P. Zhang, "Automatic Fourier transform and self-Fourier beams due to parabolic potential," *Ann. Phys.*, vol. 363, pp. 305–315, 2015.
[13] W. Liu, D. N. Neshev, I. V. Shadrivov, A. E. Miroshnichenko, and Y. S. Kivshar, "Plasmonic airy beam manipulation in linear optical potentials," *Opt. Lett.*, vol. 36, pp. 1164–1166, Apr. 2011.
[14] N. K. Efremidis, "Airy trajectory engineering in dynamic linear index potentials," *Opt. Lett.*, vol. 36, pp. 3006–3008, Aug. 2011.
[15] J. C. Guti´errez-Vega and M. A. Bandres, "Helmholtz–Gauss waves," *J. Opt. Soc. Amer. A*, vol. 22, pp. 289–298, Feb. 2005.
[16] M. A. Alonso and M. A. Bandres, "Spherical fields as nonparaxial accelerating waves," *Opt. Lett.*, vol. 37, pp. 5175–5177, Dec. 2012.
[17] I. Kaminer, R. Bekenstein, J. Nemirovsky, and M. Segev, "Nondiffracting accelerating wave packets of Maxwell's equations," *Phys. Rev. Lett.*, vol. 108, Apr. 2012, Art. no. 163901.
[18] P. Zhang *et al.*, "Generation of linear and nonlinear nonparaxial accelerating beams," *Opt. Lett.*, vol. 37, pp. 2820–2822, Jul. 2012.
[19] Y. Lumer *et al.*, "Incoherent self-accelerating beams," *Optica*, vol. 2, pp. 886–892, Oct. 2015.
[20] Y. Q. Zhang *et al.*, "Fractional nonparaxial accelerating Talbot effect," *Opt. Lett.*, vol. 41, pp. 3273–3276, Jul. 2016.
[21] P. Zhang *et al.*, "Nonparaxial Mathieu and Weber accelerating beams," *Phys. Rev. Lett.*, vol. 109, Nov. 2012, Art. no. 193901.
[22] P. Aleahmad, M.-A. Miri, M. S. Mills, I. Kaminer, M. Segev, and D. N. Christodoulides, "Fully vectorial accelerating diffraction-free helmholtz beams," *Phys. Rev. Lett.*, vol. 109, Nov. 2012, Art. no. 203902.
[23] M. A. Bandres, J. C. Gutiérrez-Vega, and S. Chávez-Cerda, "Parabolic nondiffracting optical wave fields," *Opt. Lett.*, vol. 29, pp. 44–46, Jan. 2004.
[24] C. López-Mariscal, M. A. Bandres, J. C. Gutiérrez-Vega, and S. Chávez-Cerda, "Observation of parabolic nondiffracting optical fields," *Opt. Exp.*, vol. 13, pp. 2364–2369, Apr. 2005.
[25] Y. V. Kartashov, V. V. Vysloukh, and L. Torner, "Highly asymmetric soliton complexes in parabolic optical lattices," *Opt. Lett.*, vol. 33, pp. 141–143, Jan. 2008.

[26] M. A. Bandres and B. M. Rodríguez-Lara, "Nondiffracting accelerating waves: Weber waves and parabolic momentum," *New J. Phys.*, vol. 15, 2013, Art. no. 013054.
[27] M. A. Bandres, M. A. Alonso, I. Kaminer, and M. Segev, "Three-dimensional accelerating electromagnetic waves," *Opt. Exp.*, vol. 21, pp. 13917–13929, Jun. 2013.
[28] Y. Q. Zhang *et al.*, "Three-dimensional nonparaxial accelerating beams from the transverse Whittaker integral," *Europhys. Lett.*, vol. 107, 2014, Art. no. 34001.
[29] S. López-Aguayo, Y. V. Kartashov, V. A. Vysloukh, and L. Torner, "Method to generate complex quasinondiffracting optical lattices," *Phys. Rev. Lett.*, vol. 105, Jun. 2010, Art. no. 013902.
[30] O. V. Borovkova, Y. V. Kartashov, V. E. Lobanov, V. A. Vysloukh, and L. Torner, "General quasi-nonspreading linear three-dimensional wave packets," *Opt. Lett.*, vol. 36, no. 12, pp. 2176–2178, 2011.
[31] A. Ortiz-Ambriz *et al.*, "Generation of arbitrary complex quasi-non-diffracting optical patterns," *Opt. Exp.*, vol. 21, no. 19, pp. 22221–22231, Sep. 2013.
[32] S. Yan *et al.*, "Accelerating nondiffracting beams," *Phys. Lett. A*, vol. 379, nos. 12/13, pp. 983–987, 2015.
[33] S. Yan, X. Yu, M. Li, and B. Yao, "Curved optical tubes in a 4Pi focusing system," *Opt. Exp.*, vol. 23, no. 17, pp. 22890–22897, Aug. 2015.
[34] J. Zhao, I. D. Chremmos, D. Song, D. N. Christodoulides, N. K. Efremidis, and Z. Chen, "Curved singular beams for three-dimensional particle manipulation," *Sci. Rep.*, vol. 5, 2015, Art. no. 12086.
[35] J. Baumgartl, M. Mazilu, and K. Dholakia, "Optically mediated particle clearing using airy wavepackets," *Nature Photon.*, vol. 2, pp. 675–678, 2008.
[36] P. Zhang *et al.*, "Trapping and guiding microparticles with morphing autofocusing airy beams," *Opt. Lett.*, vol. 36, pp. 2883–2885, Aug. 2011.
[37] R. Schley, I. Kaminer, E. Greenfield, R. Bekenstein, Y. Lumer, and M. Segev, "Loss-proof self-accelerating beams and their use in non-paraxial manipulation of particles' trajectories," *Nature Commun.*, vol. 5, 2014, Art. no. 5189.
[38] N. Voloch-Bloch, Y. Lereah, Y. Lilach, A. Gover, and A. Arie, "Generation of electron airy beams," *Nature*, vol. 494, pp. 331–335, 2013.
[39] S. Jia, J. C. Vaughan, and X. Zhuang, "Isotropic three-dimensional super-resolution imaging with a self-bending point spread function," *Nature Photon.*, vol. 8, pp. 302–306, 2014.
[40] R. Bekenstein, R. Schley, M. Mutzafi, C. Rotschild, and M. Segev, "Optical simulations of gravitational effects in the Newton–Schrödinger system," *Nature Phys.*, vol. 11, pp. 872–878, 2015.
[41] C. Sheng, R. Bekenstein, H. Liu, S. Zhu, and M. Segev, "Wavefront shaping through emulated curved space in waveguide settings," *Nature Commun.*, vol. 7, 2016, Art. no. 10747.
[42] I. Kaminer, J. Nemirovsky, M. Rechtsman, R. Bekenstein, and M. Segev, "Self-accelerating Dirac particles and prolonging the lifetime of relativistic fermions," *Nature Phys.*, vol. 11, pp. 261–267, 2015.
[43] Y. Hu, G. A. Siviloglou, P. Zhang, N. K. Efremidis, D. N. Christodoulides, and Z. Chen, "*Self-accelerating airy beams: Generation, control, and applications*," in *Nonlinear Photonics and Novel Optical Phenomena* (*ser. Springer Series in Optical Sciences*), Z. Chen and R. Morandotti, Eds. New York, NY, USA: Springer, 2012, vol. 170, pp. 1–46.
[44] M. A. Bandres *et al.*, "Accelerating optical beams," *Opt. Photon. News*, vol. 24, pp. 30–37, Jun. 2013.
[45] U. Levy, S. Derevyanko, and Y. Silberberg, "Light modes of free space," *Prog. Opt.*, vol. 61, pp. 237–281, 2016.
[46] Z. Chen *et al.*, "Control and novel applications of self-accelerating beams," *Acta Opt. Sin.*, vol. 36, 2016, Art. no. 1026009 (in Chinese).
[47] Y. Lumer, L. Drori, Y. Hazan, and M. Segev, "Accelerating self-imaging: The Airy-Talbot effect," *Phys. Rev. Lett.*, vol. 115, Jul. 2015, Art. no. 013901.
[48] Y. Q. Zhang *et al.*, "Dual accelerating Airy-Talbot recurrence effect," *Opt. Lett.*, vol. 40, pp. 5742–5745, Dec. 2015.
[49] E. Wolf, *Introduction to the Theory of Coherence and Polarization of Light.* Cambridge, U.K.: Cambridge Univ. Press, 2007.